I.A.U
Karaj branch

Journal of
A p p l ied
C hemical
R esearch
jacr.kiau.ac.ir

Journal of Applied Chemical Research, 18, 1, 41-59 (2024)

Fabrication of Graphene Oxide Nanocomposite Based on Poly(3-hydroxybutyrate)-Chitosan as a Useful Drug Carrier

Seyed Mohammadjafar Mousavi[1], Mirzaagha Babazadeh[1*], Mahboob Nemati[2,3], Moosa Es'haghi[1]

[1]Department of Chemistry, Tabriz Branch, Islamic Azad University, Tabriz, Iran

[2]Food and Drug Safety Research Center, Tabriz University of Medical Sciences, Tabriz, Iran

[3]Department of Pharmaceutical and Food Control, Faculty of Pharmacy, Tabriz University of Medical Sciences, Tabriz, Iran

(Received 17 May 2023; Final revised received 02 Aug. 2023)

Abstract

This research work describes a simple, eco-friendly, and facile method to synthesize a novel graphene oxide (GO) nanocomposite based on poly(3-hydroxybutyrate)-chitosan (PHB-CS) grafted to poly(methyl methacrylate-block-(poly(ethylene glycol) methacrylate-random-2-(dimethyl amino) ethyl methacrylate)) copolymer. The obtained nanocomposite was designated as GO/PHB-CS-g-P(MMA-b-(PEGMA-ran-DMAEMA)) and investigated as a drug delivery system. The synthesized products were characterized by FTIR, ^{1}HNMR, scanning electron microscopy (SEM), dynamic light scattering (DLS) and thermogravimetric analysis (TGA). Doxorubicin (DOX) as an anticancer drug was loaded on the synthesized GO nanocomposite and the drug encapsulation efficiency was calculated about 76.4%. The release profiles indicated that the resulting GO nanocomposite has a pH-responsive behavior under physiological conditions due to the hydrogen bonding interaction between PHB-CS-g-P(MMA-b-(PEGMA-ran-DMAEMA)) and GO. The release property of DOX from GO nanocomposite exhibited a slow sustained release, and suggested that the GO/PHB-CS-g-P(MMA-b-(PEGMA-ran-DMAEMA)) nanocomposite could be an appropriate candidate as a useful nanocarrier for the release of DOX in controlled drug delivery systems for treatment of cancer cells.

Keywords: Poly(3-hydroxybutyrate), Chitosan, Doxorubicin, Graphene Oxide, Nanocomposite, Drug Delivery Systems.

***Corresponding author:** *Mirzaagha Babazadeh, Department of Chemistry, Tabriz Branch, Islamic Azad University, Tabriz, Iran. E-mail: babazadeh@iaut.ac.ir*

Introduction

In recent years, drug delivery systems have attracted more attentions, which can reduce toxic side effects and optimize the selectivity of drugs [1-3]. Many drug delivery systems such as polymer-drug conjugates [4], gold nanoparticles [5, 6], graphene nanoparticles [7, 8], magnetic nanoparticles [9, 10] and carbon nanotubes [11] have been investigated for the delivery of anticancer drugs. Several properties of the ideal drug delivery systems should be concerned for successful cancer treatment such as efficient loading [12, 13], targeted delivery [14], and controlled release [15]. Nanoparticle-mediated anticancer drug delivery systems have numerous advantages, including enhanced drug accumulation in tumor tissues, increased stability of anticancer drugs in blood, the ability to be functionalized with passive, decreased systemic toxicity, and active targeted moieties [16-19].

Graphene as a two dimensional monoatomic compound is an excellent nanomaterial for drug delivery applications [20]. Graphene oxide (GO), as an ideal nanocarrier, has attracted more attention due to its excellent biocompatibility and good stability in aqueous solutions [21-23]. Also, GO has a large π-conjugated structure and a specific surface area. Drugs such as doxorubicin [24, 25], 5-fluorouracil [26], ibuprofen [27], and camptothecin [28] can be loaded onto GO *via* intrinsic van der Waals interaction and π–π stacking. In addition, carboxyl and hydroxyl functional groups on GO can be attached to the drugs *via* strong hydrogen bonds.

GO-based nanomaterials could be selected as an ideal candidate for anticancer drugs delivery because of several reasons. Firstly, the large surface area of GO provides sufficient sites for loading anticancer drugs. Secondly, the presence of abundant oxygen-containing functional groups is advisable for anticancer drugs delivering through chemical routes. Thirdly, the aromatic anticancer drugs are well-matched with the structure of GO [29].

Poly(3-hydroxybutyrate) (PHB) as a synthetic polymer is a piezoelectric, bacterially derived polymer, and biodegradable polyester with optical activity, which can stimulate bone growth [30, 31]. PHB is produced by the fermentation of sugars, lipids and other functional groups [32]. Moreover, the good mechanical properties of the PHB are suitable for repairing the soft tissues [33, 34]. PHB has good degradability and biocompatibility properties with long-duration treatment methods that are helpful for tissue regeneration such as nerve [35]. PHB is not suitable for drug delivery applications due to its hydrophobicity properties. Therefore, one of the most effective methods is coupling PHB with a natural polymer to reduce the limitations of PHB. Also, an effective technique is incorporating natural polymers with synthetic polymers to enhance the biodegradability and biocompatibility of drug delivery systems [36-39].

Chitosan (CS) as a biopolymer and natural polysaccharide is widely distributed in the exoskeleton of fungal cell wall, crustaceans, and other biological materials [40, 41]. CS has been widely reported for drug delivery applications due to its excellent biocompatibility, biodegradability, and positive characteristics [42, 43]. CS is insoluble in most organic solvents, but easily dissolves in dilute acidic solutions due to the presence of primary amino groups. The solubility of CS in water can be easily controlled by adjusting the pH value.

Library studies show that the copolymers based on PHB and chitosan are biodegradable and environmentally friendly with properties desirable for biomedical applications. In principle, CS-based graft copolymerization is investigated as a good technique to provide materials with improved properties [43].

Several reports have investigated the biosafety of graphene oxide-based nanocomposite polymers as antibacterial materials and useful carrier in drug delivery systems. Yang *et al.* [44] fabricated poly(vinyl alcohol)-chitosan/graphene oxide (PVA-CS/GO) composite nanofibers through electrospinning and manifested remarkable antibacterial activity towards *Escherichia coli* and *Staphylococcus aureus*. Huang *et al.* [45] prepared GO-polyethyleneimine hybrid films, exhibiting improved mechanical strength and displaying good antibacterial activity. Ghamkhari *et al.* [46] reported the development of termo-responsive nanocomposites from GO/(β-cyclodextrin)-star-poly(methyl methacrylate)-block-poly(*N*-isopropylacrylamide) *via* reversible addition fragmentation chain transfer (RAFT) polymerization. The drug loading efficiency of GO nanocomposites for docetaxel as an anticancer chemotherapy drug was obtained 85%. In another report, a biodegradable star-liked polymeric micelle based on poly(ε-caprolactone)-*b*-poly(*N*-isopropylacrylamide) was developed for the overcome limitations of docetaxel-loading. The docetaxel-encapsulation efficiency was calculated 95.5% and release kinetic of drug was studied under *in vitro* conditions [47].

According to our literature review, no studies have been performed to evaluate the application of GO nanocomposite based on PHB-CS-g-P(MMA-b-(PEGMA-ran-DMAEMA)) for a biomedical device or its capacity for drug delivery. Therefore, the main objective of this work is to prepare and characterize the GO/PHB-CS-g-P(MMA-b-(PEGMA-ran-DMAEMA)) nanocomposite by investigating its loading capacity and its ability to release the doxorubicin (DOX) as a chemotherapy drug under *in vitro* conditions.

Experimental

General

4-Cyano-4-[(phenylcarbothioyl) sulfanyl] pentanoic acid, as a RAFT agent was synthesized in our laboratory [47]. CS (medium molecular weight, extent of deacetylation 75–85%), PHB, 1-ethyl-3-(3-dimethylaminopropyl) carbodiimide (EDC), *N*-hydroxysuccinimide (NHS), 4-(dimethyl amino) pyridine (DMAP), and *N*,*N*-dicyclohexylcarbodiimide (DCC), graphite, sodium nitrate ($NaNO_3$), potassium permanganate ($KMnO_4$), and sulfuric acid (H_2SO_4) were purchased from Sigma-Aldrich. Doxorubicin hydrochloride (DOX) was purchased from Zhejiang Hisun Pharmaceutical Company (China). 2,2-Azobisisobutyronitrile (AIBN) and other reagents were obtained from Fluka, and purified according to standard methods. Infrared spectra were recorded with KBr discs on FTIR (Shimadzu 8101M) spectrophotometer. ^{1}HNMR spectra were recorded in deuterated dimethyl sulfoxide solvent (DMSO-d_6) on Bruker (400 MHz) instrument. The size of the nanocomposite was measured by photon correlation spectroscopy (Zetasizer Nano ZS90) at different temperatures. The morphologies of compounds were determined by using the scanning electron microscope (SEM) type 1430 VP (LEO Electron Microscopy). Thermal stabilities were investigated by thermal gravimetric analyzer (Perkin Elmer, TGA-7) under a nitrogen atmosphere (flow 35 ml/min) at heating rate of 10°C/min. The amount of the released drug was determined by Shimadzu 2100 UV-vis spectrophotometer at the maximum adsorption of doxorubicin (480 nm) in an aqueous buffered solution with a 1-cm quartz cell.

Synthesis of poly(methyl methacrylate) (PMMA)

RAFT agent (3.0 mg, 0.2 mmol), MMA monomer (3 ml, 28 mmol), AIBN (1 mg, 0.005 mmol) and DMF(10 ml) were added in a reactor. The reactor was then degassed and transferred to an oil bath at 70 °C for about 20 h. Finally, the flask was quenched and precipitated in cold diethyl ether (100 ml). The product was dried under vacuum at room temperature to obtain PMMA.

Synthesis of P(MMA-b-(PEGMA-ran-DMAEMA)) copolymer

P(MMA-b-(PEGMA-ran-DMAEMA)) copolymer was synthesized according to our previous work [48]. Briefly, macro-RAFT agent (PMMA, 0.5 g, 0.07 mmol), PEGMA (0.7 g, 5.3 mmol), DMAEMA (0.7 g, 5.3 mmol), and AIBN (1 mg, 0.005 mmol) were dissolved in DMF (5 ml). The solution was then degassed and moved in an oil bath at 75 °C for 20 h. Finally, the solution was quenched and precipitated in cold diethyl ether (100 ml). The product was dried under vacuum at room temperature to obtain copolymer.

Synthesis of poly(3-hydroxybutyrate)-N-hydroxysuccinimide (PHB-NHS)

PHB (0.5 g) in anhydrous DMF (6 ml) was converted to PHB-NHS in the presence of EDC (70 mg, 0.36 mmol) and excess NHS (38 mg, 0.33 mmol) by stirring at 25 °C for 24 h under a nitrogen atmosphere. PHB-NHS was precipitated by adding cold diethyl ether (10 ml), and dried under vacuum to remove solvent [50] (Scheme 1a).

Synthesis of poly(3-hydroxybutyrate)-chitosan (PHB-CS)

Chitosan (0.375 g, 0.11 mmol) was dissolved in acetic acid (1%), and added dropwise into PHB-NHS (50 mg) dissolved in anhydrous DMF (5 ml). The solution was stirred at room temperature for 20 h, and precipitated with cold diethyl ether. Finally, The obtained precipitate was collected and dried under vacuum at room temperature to remove solvent. (Scheme 1b).

Synthesis of PHB-CS-g-P(MMA-b-(PEGMA-ran-DMAEMA))

For this purpose, PHB-CS (0.03 mmol) and P(MMA-b-(PEGMA-ran-DMAEMA) copolymer (0.5 g, 0.03 mmol) was dissolved in DMF (20 ml) under argon atmosphere. Then DCC (0.1 g) and DMAP (0.01 g) were added to the above solution. The mixture was stirred at 25 °C for 24 h, and precipitated in cold diethyl ether (100 ml). Finally, the precipitate was dried under vacuum at room temperature (Scheme 1c).

Synthesis of GO by Hummer's method

In typical procedure, GO was produced using Hummer's method from pure graphite powder. $NaNO_3$ (1.5 g), H_2SO_4 (135 ml), and graphite powder (4 g) were added to a 250-ml flask and stirred for 50 min at 25 °C. Then, $KMnO_4$ (14 g) was slowly added to the flask and the mixture was stirred at 35 °C for 8 h. In the next step, the content was diluted by deionized water (700 ml) followed by addition of H_2O_2 (35 ml) to reduce unreacted $KMnO_4$. The final mixture was centrifuged (7000 rpm, 20 min), and the precipitate was washed with HCl (0.1 M) and distilled water to reach pH=7. Finally, GO was collected and dried at 65 °C under vacuum [49].

Synthesis of GO/PHB-CS-g-P(MMA-b-(PEGMA-ran-DMAEMA)) nanocomposite

GO (200 mg) was dispersed in DMF (20 ml) and added to PHB-CS-g-P(MMA-b-(PEGMA-ran-DMAEMA)) (200 mg). The mixture was sonicated in an ultrasound bath for 20 minutes to get well dispersed. GO/PHB-CS-g-P(MMA-b-(PEGMA-ran-DMAEMA) nanocomposite as a black dispersion was centrifuged and dried under vacuum at room temperature to obtain the final product (Scheme 2a).

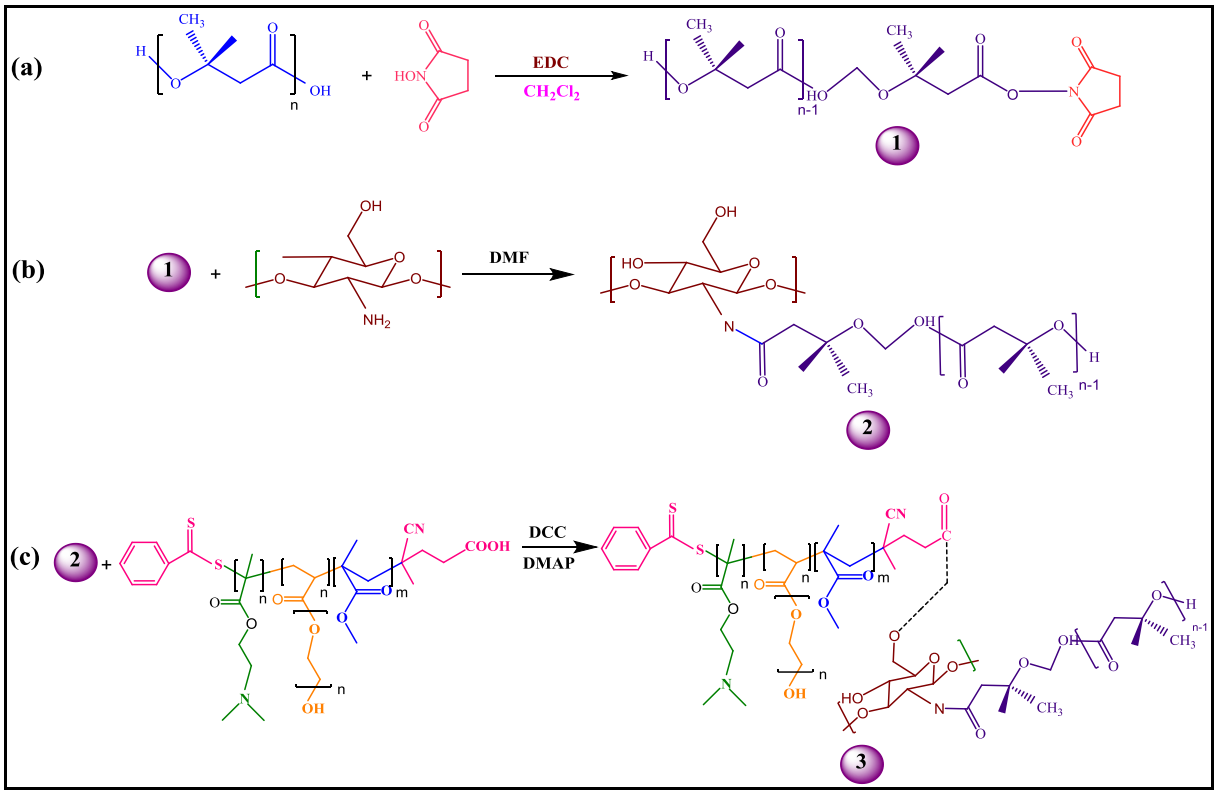

Scheme1. Synthetic route of (a) PHB-NHS, (b) PHB-CS, (c) PHB-CS-g-P(MMA-b-(PEGMA-ran-DMAEMA)).

DOX loading on the GO/PHB-CS-g-P(MMA-b-(PEGMA-ran-DMAEMA)) nanocomposite

Drug loading on the nanocomposite was done by membrane dialysis method. For this purpose, GO/PHB-CS-g-P(MMA-b-(PEGMA-ran-DMAEMA)) nanocomposite (150 mg) was dispersed in DMSO (4 ml), and treated by ultrasound waves (1.5 Hz frequency) at 25 °C. Then, DOX (15 mg) was added into the dispersed solution and stirred for 45 h under dark conditions (Scheme 2b). The solution was poured into a dialysis membrane bag and dialyzed against deionized water (200 ml) for 2 days. Then, the dispersed solution of DOX-loaded GO/PHB-CS-g-P(MMA-b-(PEGA-ran-DMAEMA)) nanocomposite was centrifuged at 6000 rpm for 15 min and the unloaded drug (supernatant phase) was analyzed by UV-vis spectrophotometry at the wavelength of 480 nm. Drug loading efficiency and drug encapsulation efficiency of DOX were calculated by the following equations:

$$\text{Drug loading efficiency (\%)} = \frac{\text{(mg of DOX in GO nanocomposite)}}{\text{(mg of GO nanocomposite)}} \times 100$$

$$\text{Drug encapsulation efficiency (\%)} = \frac{\text{(mg of DOX in GO nanocomposite)}}{\text{(mg of initial added DOX)}} \times 100$$

In vitro DOX release investigation

DOX-loaded GO/PHB-CS-g-P(MMA-b-(PEGMA-ran-DMAEMA)) nanocomposite (50 mg) was immersed in p*hosphate-buffered saline* (PBS) medium with various pH values (pH= 5.4 and 7.4), and stirred at 300 rpm individually at 37 °C. Then, 2 ml of PBS solution was centrifuged at different times and a fresh PBS solution was poured into the sample. The quantity of the released DOX was detected with a UV-vis spectrophotometer at 480 nm, and determined from the calibration curve obtained previously under the same conditions.

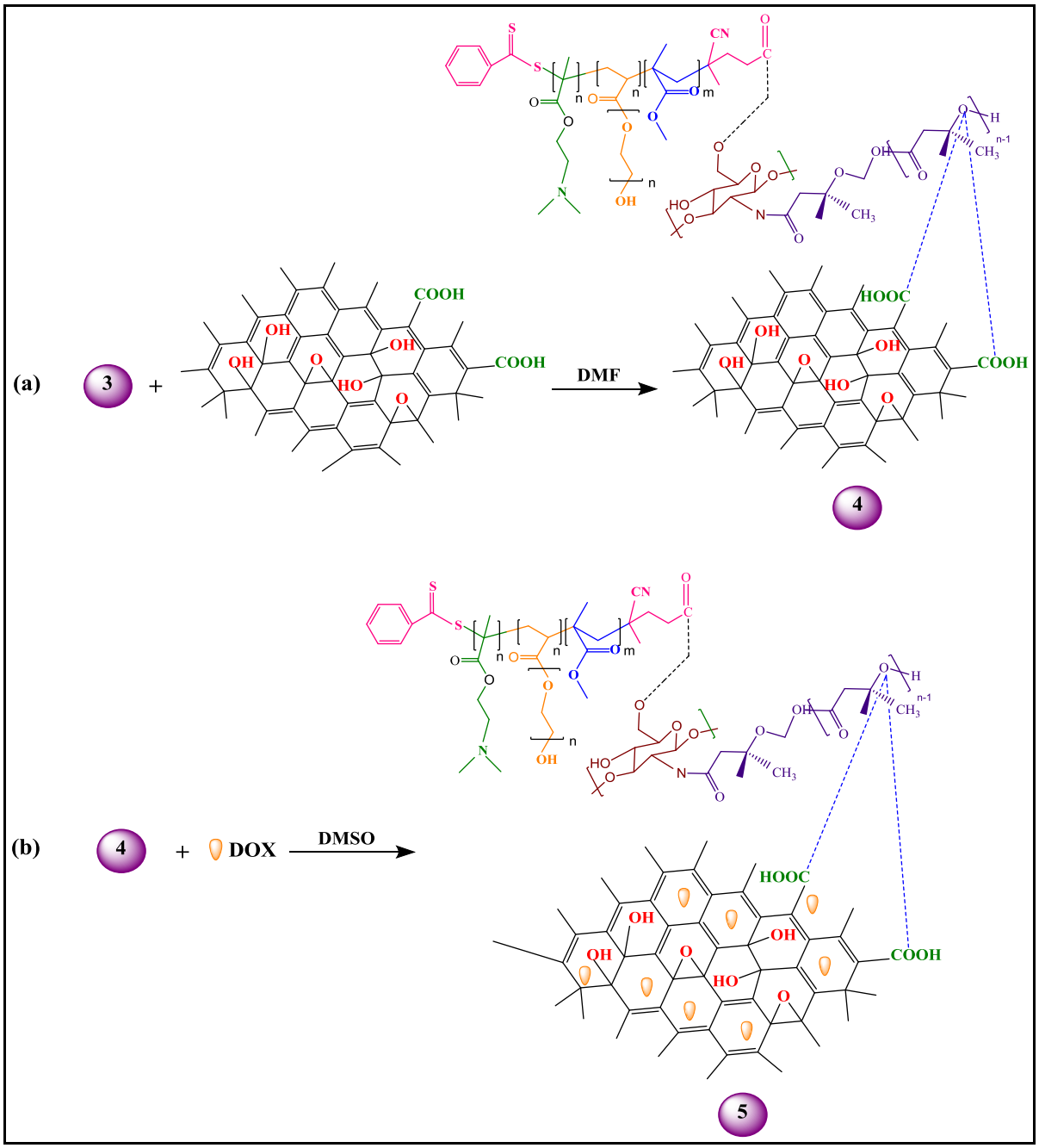

Scheme 2. Synthetic route of (a) GO/PHB-CS-g-P(MMA-b-(PEGMA-ran-DMAEMA)) nanocomposite, and (b) DOX-loaded GO/PHB-CS-g-P(MMA-b-(PEGMA-ran-DMAEMA)).

Result and discussion

FTIR spectra of the PHB, CS, P(MMA-b-(PEGMA-ran-DMAEMA)) and PHB-CS-g-P(MMA-b-(PEGMA-ran-DMAEMA)) are displayed in Figure 1. In the FTIR spectrum of PHB, the most relevant peak relates to the stretching vibrations of the carbonyl groups (O-C=O) was shown at 1725 cm^{-1} (Figure 1a). In the spectrum of chitosan, various bands were demonstrated that the first peak could be seen at 3350 cm^{-1}, representing N-H and O-H bonds. Also, the stretching vibrations of the aromatic and aliphatic C-H bonds are seen at 2900-2850 cm^{-1} region. The bending vibrations of NH groups are observed at 1600 cm^{-1} while the C-O-C glycosidic linkage is seen at 1100 cm^{-1} (Figure 1b). In the FTIR spectrum of P(MMA-*b*-(PEGMA-ran-DMAEMA)), the stretching vibrations of carbonyl and OH groups are seen at 1732 and 3442 cm^{-1}, respectively (Figure 1c). The main absorption bands in the FTIR spectrum of PHB-CS-g-P(MMA-b-(PEGMA-ran-DMAEMA)) were introduced at 1730, 2928, and 3500 cm^{-1} which correspond to the stretching vibrations of carbonyl groups, C-H bonds, and O-H groups, respectively (Figure 1d).

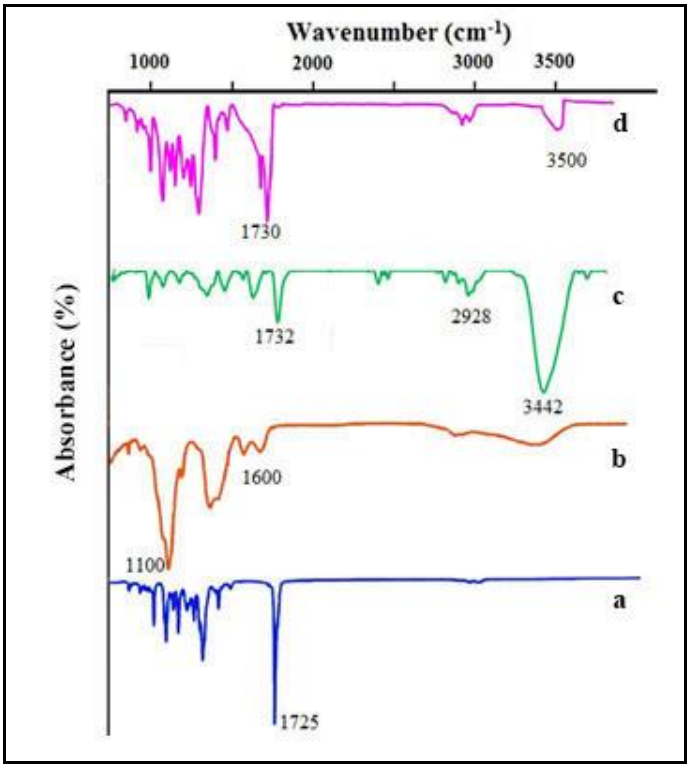

Figure 1. FTIR spectra of (a) PHB, (b) chitosan, (c) P(MMA-b-(PEGMA-ran-DMAEMA)), and (d) PHB-CS-g-P(MMA-b-(PEGMA-ran-DMAEMA)).

The FTIR spectra of GO and GO/PHB-CS-g-P(MMA-b-(PEGMA-ran-DMAEMA)) nanocomposite are shown in Figure 2. The FTIR spectrum of GO shows the presence of sharp bands at 1710 cm^{-1} (for C=O stretching), 1650 cm^{-1} (for C=C stretching), 1250 cm^{-1} (for C-O-C stretching), 1080 cm^{-1}

(for C-O stretching), 3500 and 1380 cm^{-1} for hydroxyl group deformation peak (Figure 2a). These band positions indicate the presence of oxygen containing moieties such as carbonyl, carboxylic, epoxy, and hydroxyl in graphene oxide. The FTIR spectrum of GO/PHB-CS-g-P(MMA-b-(PEGMA-ran-DMAEMA)) nanocomposite shows the characteristic absorption bands attributable to the C-O-C stretching vibration at 1260 cm^{-1}, stretching vibrations of C-O groups of the epoxy and carboxylic acid at 1050 cm^{-1}, carbonyl stretching vibration at 1700 and 1725 cm^{-1}, and hydroxyl groups stretching vibration at 3490 cm^{-1}, respectively (Figure 2b).

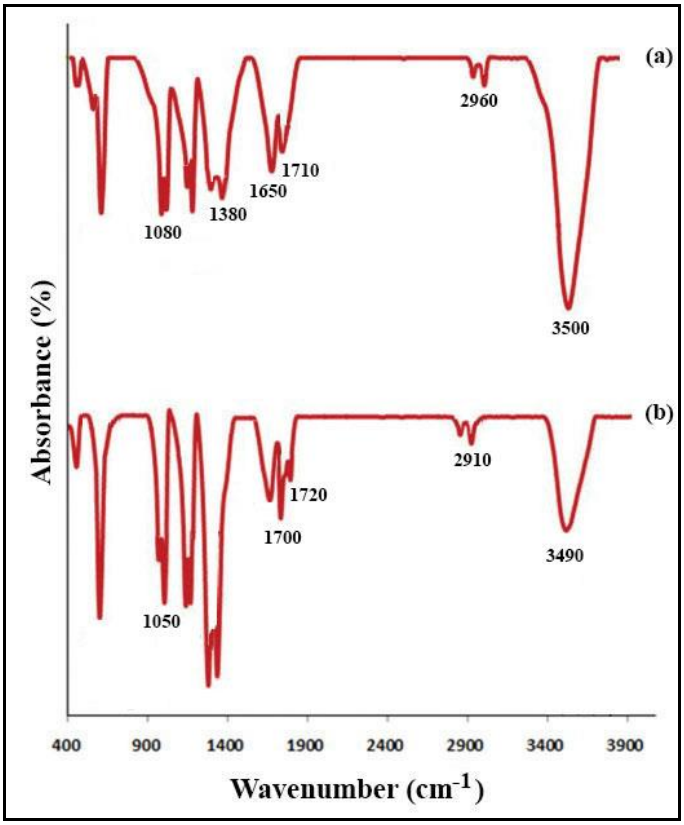

Figure 2. FTIR spectra of (a) GO, and (b) GO/PHB-CS-g-P(MMA-b-(PEGMA-ran-DMAEMA)).

The successful synthesis of PHB-CS-g-P(MMA-b-(PEGMA-ran-DMAEMA)) was studied by ^{1}HNMR spectroscopy as shown in Figure 3. In this ^{1}HNMR spectrum, the chemical shifts at 1 ppm and 1.9 ppm were assigned to the methyl (CH_3) and methine ($CH\text{-}CH_3$) protons of the PHB. The chemical shifts of ($N\text{-}CH_3$) and ($O\text{-}CH_3$) protons are seen at 2.2 and 3.8 ppm. The protons of chitosan were assigned at 3.5 ppm. Furthermore, the chemical shift at 7-8 ppm is related to the aromatic protons of RAFT agent.

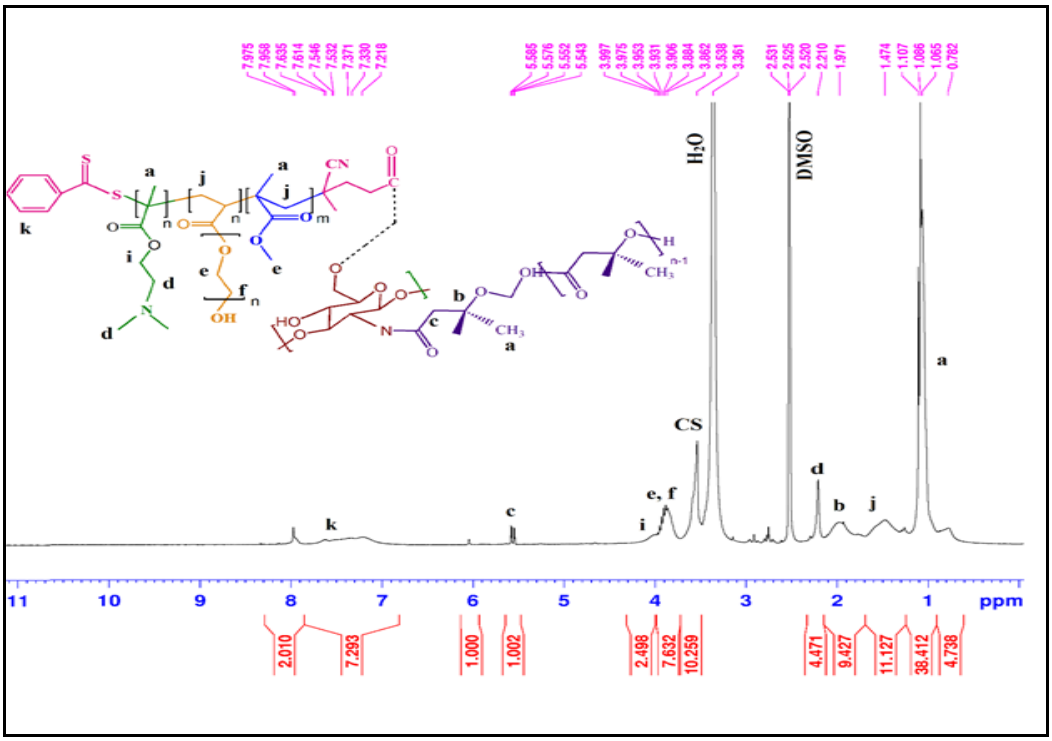

Figure 3. [1]HNMR spectrum of the PHB-CS-g-P(MMA-b-(PEGMA-ran-DMAEMA)) in DMSO-d_6 (400 MHz).

The morphology of GO and GO/PHB-CS-g-P(MMA-b-(PEGMA-ran-DMAEMA)) nanocomposite were characterized by SEM instrument (Figure 4). The synthesized GO has a sheet-like structure with a smooth surface and wrinkled edge (Figure 4a). As shown in Figure 4b, surface morphology of GO/PHB-CS-g-P(MMA-b-(PEGMA-ran-DMAEMA)) nanocomposite is different from that of GO. A relatively coarse and dense surface containing many wrinkles was observed on the surface of the nanocomposite, indicating that the GO has been covered with PHB-CS-g-P(MMA-b-(PEGMA-ran-DMAEMA)) chains.

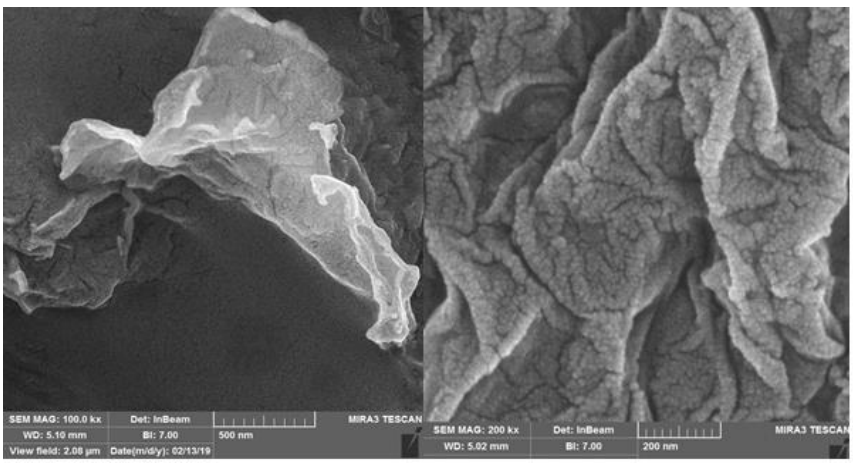

(a) **(b)**

Figure 4. SEM images of (a) GO, and (b) GO/PHB-CS-g-P(MMA-b-(PEGMA-ran-DMAEMA)) nanocomposite.

The thermal stability of GO, PHB-CS and GO/PHBCS-g-P(MMA-b-(PEGMA-ran-DMAEMA)) was studied using TGA instrument (Figure 5). A high weight loss (78 wt%) between 270-320 °C in the PHB-CS mass losses indicates degradation of the PHB and CS contained. It should be noted that PHB is almost degraded at 275 °C, with maximized degradation at 320 °C, which in this stage about 90% of PHB is lost. This matter is confirmed by previous articles [51, 52]. The GO mass losses occurred in a three-step process. The weight loss in the first step below 100 °C in the range of 21 wt% was attributed to the evaporation of intercalated water molecules. The second step was measured between 110-230 °C to be 33 wt% due to the CO_2, CO and steam release from the functional groups. The third step was observed between 230-320 °C in the range of 12.5 wt % due to the degradation of stable oxygen functionalities. The presence of PHB-CS-g-P(MMA-b-(PEGMA-ran-DMAEMA)) in GO nanosheets causes the degradation rate to be slightly enhanced. With increasing temperature, a weight loss of 23.5 w% is observed between 110-240 °C. The significant degradation between 220-500 °C with a weight loss of 36 wt% could be attributed to the decomposition of the synthesized GO nanocomposite. This evidence showed that PHB-CS-g-P(MMA-b-(PEGMA-ran-DMAEMA)) has been functionalized on the GO nanosheets.

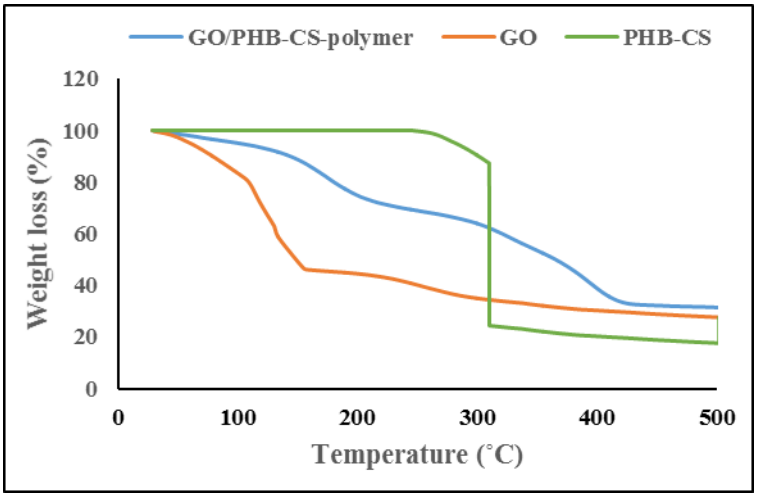

Figure 5. TGA curves of GO, PHB-CS and GO/CS-g-P(MMA-b-(PEGMA-ran-DMAEMA)) nanocomposite.

The particle size of GO/PHB-CS-g-P(MMA-b-(PEGMA-ran-DMAEMA)) nanocomposite was measured by DLS, and obtained about 150 nm (Fig. 6). To confirm the polymer coupling, we used zeta potential analysis. The zeta potential of free GO was about -33 mV [53] and after the coupling PHB-CS-g-P(MMA-b-(PEGMA-ran-DMAEMA)) to GO, the zeta potential changed from negative to positive (-16.7 mV) (Fig. 6). This result confirmed that PHB-CS-g-P(MMA-b-(PEGMA-ran-DMAEMA)) has been successfully attached to the surface of GO.

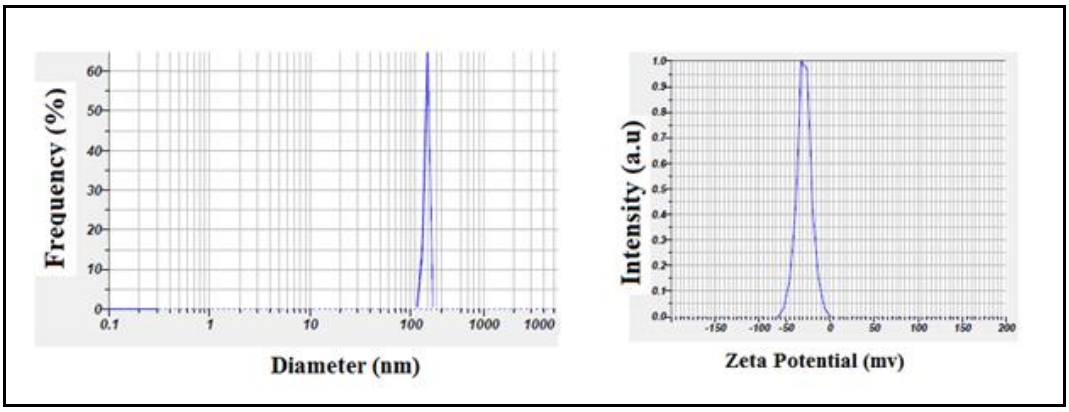

Figure 6. Particle size and zeta potential of GO/PHB-CS-g-P(MMA-b-(PEGMA-ran-DMAEMA)).

The drug carriers are designed to achieve a high drug-loading capacity. The drug loading capacity of the synthesized nanocomposite was investigated by UV-vis spectrophotometry at 480 nm. DOX encapsulation efficiency and the drug loading content were calculated about 76.4% and 6.78%, respectively. Compared with other drug delivery systems, GO has epoxy and hydroxyl groups on the sp^3 hybridized carbon that the interaction between DOX and GO could be conjugated *via* π-π staking. Also, hydrogen bonding may occur between the COOH, and OH groups of GO with the NH_2 and OH groups of DOX. For this purpose, the GO/PHB-CS-g-P(MMA-b-(PEGMA-ran-DMAEMA)) was fabricated.

The release performance of DOX-loaded GO/PHB-CS-g-P(MMA-b-(PEGMA-ran-DMAEMA)) nanocomposite at pH=5.4 and pH=7.4 (37 °C) after 100 h was 33.9% and 21.4%, respectively. The release rate of DOX from DOX-loaded nanocomposite is considerably simulated by differences in local pH as demonstrated in Figure 7, where the percentage of drug released into PBS (pH 5.4 and 7.4) is plotted as a function of time. The release property of DOX-loaded nanocomposite exhibited a slow sustained release contrasted with the free DOX solution. Although 10% of the DOX-loaded on the nanocomposite was released in the primary 4 h, but the fast release would not impact the drug safety. Also, it was seen that the release profile is pH-responsive. The drug release rate from nanocomposite is stable under normal physiological conditions, but drug release under acidic conditions is important in clinical situations (cancerous tissue environment). The release rate of DOX at pH 7.4 (37 °C) was relatively low and released about 21.4% after 100 h. At this pH, a strong ionic interaction exists between DOX and GO nanocomposite due to the protonation of DOX (positive charge) and deprotonation of the amine group of PDMAEMA (negative charge). The release rate of DOX at pH 5.4 (37 °C) was accelerated and released about 33.9% after 100 h. At this pH, ionic interaction between DOX and nanocomposite disappeared.

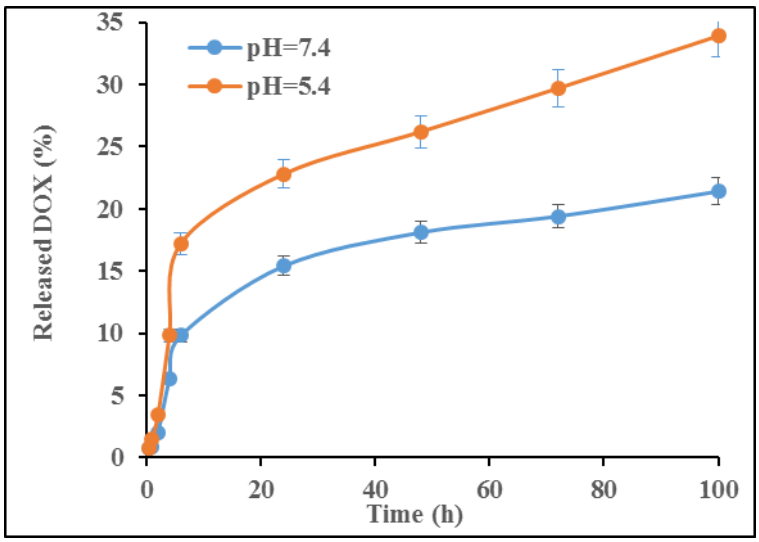

Figure 7. In vitro release profiles of DOX from nanocomposite at various pH media (37 °C).

Conclusion

In this study, we designed a drug delivery system based on GO nanocomposite to obtain a useful nanocarrier for the controlled release of DOX. GO was functionalized with PHB-CS-g-P(MMA-b-(PEGMA-ran-DMAEMA)) and DOX was then linked onto its surface using electrostatic interactions. Exceptional capacity for drug loading, excellent encapsulation efficiency, and responsiveness to pH are the characteristics of the synthesized GO nanocomposite. The release studies showed that the release of DOX from GO nanocomposite is slower at acidic pH than at physiological pH. The obtained results suggest that the synthesized GO nanocomposite could be further studied as a potential nanocarrier for chemotherapy drugs in the treatment of cancer cells that have lower pH than normal cells.

Acknowledgement

The authors would like to thank Tabriz Branch, Islamic Azad University for the support of this research.

References

1. Adeli F., Abbasi F., Babazadeh M., Davaran S. Thermo/pH dual-responsive micelles based on the host-guest interaction between benzimidazole-terminated graft copolymer and β-cyclodextrin-functionalized star block copolymer for smart drug delivery. J Nanobiotech. 2022;20:91.

2. Samadzadeh S., Babazadeh M., Zarghami N., Pilevar-Sultanahmadi Y., Mousazadeh H. An

implantable smart hyperthermia nanofiber with switchable, controlled and sustained drug release: possible application in prevention of cancer local recurrence. Mater Sci Eng C. 2021;118:111384.

3. Deng S., Gigliobianco M.R., Censi R., Martino P.D. Polymeric nanocapsules as nanotechnological alternative for drug delivery system: current status, challenges and opportunities. Nanomater. 2020;10(5):847.

4. Alven S., Nqoro X., Buyana B., Aderibigbe B.A. Polymer-drug conjugate, a potential therapeutic to combat breast and lung cancer. Pharmaceutics. 2020;12(5):406.

5. Zhang J., Mou L., Jiang X. Surface chemistry of gold nanoparticles for health-related applications. Chem Sci. 2020;11(4):923-36.

6. Fan M., Han Y., Gao S., Yan H., Cao L., Li Z., Liang X.J., Zhang J. Ultrasmall gold nanoparticles in cancer diagnosis and therapy. Theranostics. 2020;10(11):4944-57.

7. Rahdar A., Hajinezhad M.R., Hamishekar H., Ghamkhari A., Kyzas G.Z. Copolymer/graphene oxide nanocomposites as potential anticancer agents. Polym Bull. 2021;78(9):4877-98.

8. Ghamkhari A., Abbaspour-Ravasjani S., Talebi M., Hamishehkar H., Hamblin M.R., Development of a graphene oxide-poly lactide nanocomposite as a smart drug delivery system. Inter J Biol Macromol. 2021;169:521-31.

9. Massoumi B., Taghavi N., Ghamkhari A. Synthesis of a new biodegradable system based on β-cyclodextrin/iron oxide nanocomposite: application for delivery of docetaxel. Polym Bull. 2021;78(6):3055-70.

10. Li K., Lu L., Xue C., Liu J., He Y., Zhou J., Xia Z., Dai L., Luo Z., Mao Y., Cai K. Polarization of tumor-associated macrophage phenotype via porous hollow iron nanoparticles for tumor immunotherapy in vivo. Nanoscale. 2020;12(1):130-44.

11. Anzar N., Hasan R., Tyagi M., Yadav N., Narang J. Carbon nanotube-a review on synthesis, properties and plethora of applications in the field of biomedical science. Sens Inter. 2020;1:100003.

12. Samadzadeh S., Mousazadeh H., Ghareghomi S., Dadashpour M., Babazadeh M., Zarghami N. In vitro anticancer efficacy of Metformin-loaded PLGA nanofibers towards the post-surgical therapy of lung cancer. J Drug Deliv Sci Technol. 2021;61:102318.

13. Mohebian Z., Babazadeh M., Zarghami N., Mousazadeh H. Anticancer efficiency of curcumin-loaded mesoporous silica nanoparticles/nanofiber composites for potential postsurgical breast cancer treatment. J Drug Deliv Sci Technol. 2021;61:102170.

14. Rad F., Davaran S., Babazadeh M., Akbarzadeh A., Pazoki-Torodi H. Biodegradable

electrospun polyester-urethane nanofiber scaffold: co-delivery investigation of doxorubicin-ezetimibe and its synergistic effect on prostate cancer cell line. J Nanomater. 2022;2022:8818139.

15. Mikula K., Izydorczyk G., Skrzypczak D., Mironiuk M., Moustakas K., Witek-Krowiak A., Chojnacka K. Controlled release micronutrient fertilizers for precision agriculture-a review. Sci Total Environ. 2020;712:136365.

16. Bayer I.S. Hyaluronic acid and controlled release: a review. Molecules. 2020;25(11):2649.

17. Yalcin T.E., Ilbasmis-Tamer S., Takka S. Antitumor activity of gemcitabine hydrochloride loaded lipid polymer hybrid nanoparticles (LPHNs): in vitro and in vivo. Inter J Pharm. 2020;580:119246.

18. Wang X., Wang Y., Hu J., Xu H. An antitumor peptide RS17-targeted CD47, design, synthesis, and antitumor activity. Cancer Med. 2021;10(6):2125-36.

19. Inchina V.I., Izbastyyeva M.D., Tarasova T.V., Ulanova T.V., Avanesov A.M., Khaydar D.A. Antitumor efficacy of liposomal doxorubicin hydrochloride in combination with tamoxifen: experimental study. Archiv Euromedica. 2020;10(3):22-4.

20. Wang Z., Peng P., Zhang L., Wang N., Tang B., Cui B., Liu J., Xu D. Effect of electric field on the microstructure and electrical properties of (In+Ta) co-doped TiO_2 colossal dielectric ceramics. J Mater Sci Mater Electron. 2022;33(9):6283-93.

21. Karki N., Tiwari H., Tewari C., Rana A., Pandey N., Basak S., Sahoo N.G. Functionalized graphene oxide as a vehicle for targeted drug delivery and bioimaging applications. J Mater Chem B. 2020;8(36):8116-48.

22. Ashjaran M., Babazadeh M., Akbarzadeh A., Davaran S., Salehi R. Stimuli-responsive polyvinylpyrrolidone-NIPPAm-lysine graphene oxide nano-hybrid as an anticancer drug delivery on MCF7 cell line. Artif Cells Nanomed Biotechnol. 2019;47(1):443-54.

23. Cha-umpong W., Mayyas M., Razmjou A., Chen V. Modification of GO-based pervaporation membranes to improve stability in oscillating temperature operation. Desalination. 2021;516:115215.

24. Mahdavi M., Fattahi A., Tajkhorshid E., Nouranian S. Molecular insights into the loading and dynamics of doxorubicin on PEGylated graphene oxide nanocarriers. ACS Appl Bio Mater. 2020;3(3):1354-63.

25. Borandeh S., Hosseinbeigi H., Abolmaali S.S., Monajati M., Tamaddon A.M. Steric stabilization of β-cyclodextrin functionalized graphene oxide by host-guest chemistry: a versatile supramolecule for dual-stimuli responsive cellular delivery of doxorubicin. J Drug Deliv Sci Technol. 2021;63:102536.

26. Ashjaran M., Babazadeh M., Akbarzadeh A., Davaran S., Salehi R. A lysine functionalized graphene oxide based nanoplatform for delivery of fluorouracil to A549 human lung cancer cells: a comparative study. Tanaffos. 2021;20(4):353-62.
27. Esba L.C.A., Alqahtani R.A., Thomas A., Shamas N., Alswaidan L., Mardawi G. Ibuprofen and NSAID use in COVID-19 infected patients is not associated with worse outcomes: a prospective cohort study. Infect Dis Ther. 2021;10(1):253-68.
28. Wang F., Su H., Xu D., Dai W., Zhang W., Wang Z., Anderson C.F., Zheng M., Oh R., Wan F., Cui H. Tumour sensitization via the extended intratumoural release of a STING agonist and camptothecin from a self-assembled hydrogel. Nat Biomed Eng. 2020;4(11):1090-101.
29. Jiang C., Zhao H., Xiao H., Wang Y., Liu L., Chen H., Shen C., Zhu H., Liu Q. Recent advances in graphene-family nanomaterials for effective drug delivery and phototherapy. Expert Opin Drug Deliv. 2021;18(1):119-38.
30. Koch M., Berendzen K.W., Forchhammer K. On the role and production of polyhydroxybutyrate (PHB) in the cyanobacterium Synechocystis sp. PCC 6803. Life. 2020;10(4):47.
31. Smith M.K., Paleri D.M., Abdelwahab M., Mielewski D.F., Misra M., Mohanty A.K. Sustainable composites from poly (3-hydroxybutyrate) (PHB) bioplastic and agave natural fibre. Green Chem. 2020;22(12):3906-16.
32. Situmorang M.L., Suantika G., Santoso M., Khakim A., Wibowo I., Aditiawati P. Poly-β-hydroxybutyrate (PHB) improves nursery-phase pacific white shrimp litopenaeus vannamei defense against vibriosis. N Am J Aquac. 2020;82(1):108-14.
33. Parvizifard M., Karbasi S. Physical, mechanical and biological performance of PHBchitosan/MWCNTs nanocomposite coating deposited on bioglass based scaffold: potential application in bone tissue engineering. Int J Biol Macromol. 2020;152:645-62.
34. Panaitescu D.M., Nicolae C.A., Gabor A.R., Trusca R. Thermal and mechanical properties of poly (3-hydroxybutyrate) reinforced with cellulose fibers from wood waste. Ind Crops Prod. 2020;145:112071.
35. Liang Q., Shuping G., Chenyu L., Dongyu J., Guixue W., Tieying Y. Impact of a bioactive drug coating on the biocompatibility of magnesium alloys. J Mater Sci. 2020;55(14):6051-64.
36. Gorrasi G., Longo R., Viscusi G. Fabrication and characterization of electrospun membranes based on poly(ε-caprolactone), poly(3-hydroxybutyrate) and their blend for tunable drug delivery of curcumin. Polymers. 2020;12(10):2239.

37. Karimi Tar A., Karbasi S., Naghashzargar E., Salehi H. Biodegradation and cellular evaluation of aligned and random poly (3-hydroxybutyrate)/chitosan electrospun scaffold for nerve tissue engineering applications. Mater Technol. 2020;35(2):92-101.
38. Zhorina L.A., Iordanskii A.L., Rogovina S.Z., Grachev A.V., Yakhina A.R., Prut E.V., Berlin A.A. Thermal characterization and sorption of Feiii ion by ternary polylactide-poly-3-hydroxybutyrate-chitosan compositions. Mendeleev Commun. 2021;31(1):104-6.
39. Shoari S.A., Jafarpour A., Bagheri R., Norouzi F., Mahin T., Taherzadeh S., Allahgholipour E., Arjang S., Soleimani S., Davari Asl A., Olyayee F.F.B., Rezaei Y., Maleki Dizaj S., Sharifi S. Polymeric nano-biomaterials in regenerative endodontics. Eurasian Chem Commun. 2021;3:56-69.
40. Kumar D., Gihar S., Shrivash M.K., Kumar P., Kundu P.P. A review on the synthesis of graft copolymers of chitosan and their potential applications. Int J Biol Macromol. 2020;163:2097-112.
41. Deng W., Tang S., Zhou X., Liu Y., Liu S., Luo J. Honeycomb-like structure-tunable chitosan-based porous carbon microspheres for methylene blue efficient removal. Carbohydr Polym. 2020;247:116736.
42. Andonegi M., Heras K.L., Santos-Vizcaino E., Igartua M., Hernandez R.M., Caba K.D.L., Guerrero P. Structure-properties relationship of chitosan/collagen films with potential for biomedical applications. Carbohydr Polym. 2020;237:116159.
43. Salama A., Hasanin M., Hesemann P. Synthesis and antimicrobial properties of new chitosan derivatives containing guanidinium groups. Carbohydr Polym. 2020;241:116363.
44. Yang S., Lei P., Shan Y., Zhang D. Preparation and characterization of antibacterial electrospun chitosan/poly (vinyl alcohol)/graphene oxide composite nanofibrous membrane. Appl Surf Sci. 2018;435:832-40.
45. Huang T., Zhang L., Chen H., Gao C. A cross-linking graphene oxide-polyethyleneimine hybrid film containing ciprofloxacin: one-step preparation, controlled drug release and antibacterial performance. J Mater Chem B. 2015;3(8):1605-11.
46. Ghamkhari A., Abbasi F., Abbasi E., Ghorbani M. A novel thermo-responsive system based on β-cyclodextrin-nanocomposite for improving the docetaxel activity. Int J Polym Mater Polym Biomater. 2021;70(12):830-40.
47. Ghamkhari A., Sarvari R., Ghorbani M., Hamishehkar H. Novel thermoresponsive starliked nanomicelles for targeting of anticancer agent. Eur Polym J. 2018;107:143-54.
48. Mousavi S.M., Babazadeh M., Nemati M., Es'haghi M. Doxorubicin-loaded

biodegradable chitosan-graphene nanosheets for drug delivery applications. Polym Bull. 2022;79(8):6565-80.

49. Jankovsky O., Marvan P., Novacek M., Luxa J., Mazanek V., Klimova K., Sedmidubsky D., Sofer Z. Synthesis procedure and type of graphite oxide strongly influence resulting graphene properties. Appl Mater Today. 2016;4:45-53.

50. Sanna V., Pintus G., Bandiera P., Anedda R., Punzoni S., Sanna B., Sechi M. Development of polymeric microbubbles targeted to prostate-specific membrane antigen as prototype of novel ultrasound contrast agents. Mol Pharm. 2011;8(3):748-57.

51. Hassan M.A., Bakhiyet E.K., Ali S.G., Hussien H.R. Production and characterization of polyhydroxybutyrate (PHB) produced by Bacillus sp. isolated from Egypt. J App Pharm Sci. 2016;6(4):46-51.

52. Hosokawa M.N., Darros A.B., Moris V.A.D., Paiva J.M.F.D. Polyhydroxybutyrate composites with random mats of sisal and coconut fibers. Mater Res. 2016;20:279-90.

53. Konkena B., Vasudevan S. Understanding aqueous dispersibility of graphene oxide and reduced graphene oxide through pK_a measurements. J Phys Chem Lett. 2012;3(7):867-72.